

Non-local correlation and entanglement of ultracold bosons in the two-dimensional Bose-Hubbard lattice at finite temperature

Ulli Pohl, Sayak Ray*, and Johann Kroha

Physikalisches Institut, Rheinische Friedrich-Wilhelms-Universität Bonn, Nußallee 12, 53115, Bonn, Germany
Email: ulli.pohl@uni-bonn.de, sayak@uni-bonn.de, kroha@th.physik.uni-bonn.de

Keywords: *Cold gases in optical lattices, Bose-Hubbard model, Cluster mean-field theory, Phase diagram, Superfluid*

We investigate the temperature-dependent behavior emerging in the vicinity of the superfluid (SF) to Mott-insulator (MI) transition of interacting bosons in a two-dimensional optical lattice, described by the Bose-Hubbard model. The equilibrium phase diagram at finite-temperature is computed using the cluster mean-field (CMF) theory including a finite-cluster-size-scaling. The SF, MI, and normal fluid (NF) phases are characterized as well as the transition or crossover temperatures between them are estimated by computing physical quantities such as the superfluid fraction, compressibility and sound velocity using the CMF method. We find that the non-local correlations included in a finite cluster, when extrapolated to infinite size, leads to quantitative agreement of the phase boundaries with quantum Monte Carlo (QMC) results as well as with experiments. Moreover, we show that the von Neumann entanglement entropy within a cluster corresponds to the system's entropy density and that it is enhanced near the SF-MI quantum critical point (QCP) and at the SF-NF boundary. The behavior of the transition lines near this QCP, at and away from the particle-hole (p-h) symmetric point located at the Mott-tip, is also discussed. Our results obtained by using the CMF theory can be tested experimentally using the quantum gas microscopy method.

1 Introduction

The physics of strong correlation and entanglement in interacting quantum systems has been a focus of research in condensed matter and statistical physics for a long time, covering a broad area ranging from equilibrium to out-of-equilibrium phenomena [1–6]. In recent years, ultracold atomic systems have become an ideal platform to explore this field of research due to the fine-tunability of system parameters, so that various correlated model Hamiltonians exhibiting a quantum phase transition can be realized [7]. Recent experimental tools and imaging techniques have enabled to explore the density profiles of ultracold atoms with single-lattice-site resolution [8, 9], as well as have provided access to *in situ* measurements of local observables such as density, density fluctuation, correlation functions and entanglement [10–14]. These developments have opened an avenue to analyze the strongly correlated phases, phase transitions and non-equilibrium dynamics using cold atom systems.

The Bose-Hubbard model (BHM) is known for its success to describe the phases and dynamics of ultracold interacting bosons in a lattice [15, 16]. Its experimental realization in an optical lattice led to the landmark demonstration of the superfluid (SF) to Mott insulator (MI) phase transition [17] and its subsequent observations [18, 19]. Over the past few decades, a number of theoretical studies have investigated the different phases of the BHM at zero or the lowest possible temperature by means of different methods [20–41]. The universal conductivity at the SF-MI phase transition in two dimension has also been analyzed in a quantum Monte Carlo

(QMC) study and by using the AdS/CFT correspondence [42, 43]. The single-particle spectra in the different phases, for instance the particle-hole (p-h) excitation gap in the Mott insulator, as well as collective modes, like the gapless Goldstone mode and the massive Higgs mode in the superfluid phase, have been calculated [44–48], and their existence have been detected in cold-atom experiments for bosonic and fermionic gases [49, 50].

The behavior at finite temperatures is far less explored. There, apart from an incompressible MI and a compressible SF phase, a normal fluid (NF) with vanishing superfluidity but finite compressibility appears as a consequence of a transition from the superfluid or a crossover from the Mott insulator, respectively [15]. The SF-NF transition and the behavior of other thermodynamic quantities have been investigated in a few theoretical studies [51–58]. Experimentally, the reduction of T_c near the QCP has been observed across a vacuum-to-superfluid transition [11, 12] and across the MI-SF transition at a constant particle density (particle number per lattice site) $\bar{n} = 1$ [59]. However, a systematic analysis on the effect of correlation at low temperature is lacking, particularly in 2D systems where simple mean-field and perturbative methods fail due to enhanced fluctuations, as well as exact solution methods like density matrix renormalization group (DMRG) are not easily available.

In this paper we primarily investigate the effect of non-local correlation at low temperature in the two-dimensional Bose-Hubbard model by means of a computationally inexpensive approach, namely, the cluster mean-field (CMF) theory [60–69]. The finite-size clusters used in the CMF method incorporate spatial correlation which is beyond the scope of single site mean-field theory, as well as the single site bosonic dynamical mean-field theory (B-DMFT) where dynamical fluctuations are incorporated locally [34, 35]. We extend the CMF method to finite temperature, and study, particularly, the SF–NF transition, characterized by the superfluid transition temperature T_c , and the MI–NF crossover, characterized by the crossover temperature T^* near the QCP, both at and away from the p-h symmetry point of the BHM. While the latter one is the generic transition achieved by keeping the chemical potential fixed, the former one is a special case where the average particle number per lattice site is kept fixed at $\bar{n} = 1$. The equilibrium phase diagram is computed for both the cases. As one might expect from any MF like methods, also CMF method can not capture the behavior in the critical region of the Berezinskii–Kosterlitz–Thouless (BKT) transition relevant for the model at hand [70–72]. Our main results, as an application of the CMF method to the paradigmatic BHM in 2D at finite temperature are summarized below.

(I) We show that the method, after an appropriate cluster-size scaling, quantitatively reproduces the phase boundaries and also their associated critical exponents in agreement with the QMC results,

specifically from Refs. [31, 33, 56].

(II) We calculate the relevant physical quantities such as superfluid fraction, sound velocity and compressibility using the CMF method. Compressibility provides access to the non-local density correlations and to the particle and hole excitation gaps in the MI phase which agree quantitatively with the experiment in Ref. [49].

(III) We further compute the von Neumann entanglement entropy within a cluster, namely, *cluster entanglement entropy* (CEE), exhibiting enhancement near the QCP and at the SF-NF boundary. We show that the CEE corresponds to the system's entropy density, and thereby, it provides a robust signature of the transition.

Our theoretical results are also consistent with the experimental findings in the vicinity of the density-induced vacuum-to-superfluid transition [11, 12].

The paper is organized as follows. In Sec. 2 we introduce the BHM and explain the CMF technique. Next, in Sec. 3 we present the finite temperature phase diagram and discuss the behavior of T_c/U and T^*/U near the QCP for a generic, non-p-h symmetric MI-SF transition. This is followed by the estimation of the Mott gap and comparison with QMC and experimental results in Sec. 4.1. The behavior of the phase boundaries at the p-h symmetric multicritical point is discussed in Sec. 4.2. Finally, we summarize and conclude in Sec. 5.

2 Model and Method

2.1 The Bose-Hubbard model

The BHM within a single band and tight-binding approximation can be described by the Hamiltonian,

$$\hat{\mathcal{H}} = - \sum_{\langle i,j \rangle} (t \hat{a}_i^\dagger \hat{a}_j + \text{h.c.}) - \sum_i \left[\mu \hat{n}_i + \frac{U}{2} \hat{n}_i (\hat{n}_i - 1) \right] \quad (1)$$

where \hat{a}_i^\dagger (\hat{a}_i) are the bosonic creation (annihilation) operators at the i th site, \hat{n}_i represents the local number operator, t is the hopping amplitude between the nearest neighbor (NN) sites of a square lattice denoted by $\langle i, j \rangle$, U and μ are the onsite interaction, and the chemical potential respectively. In this paper we set the Planck constant $\hbar = 1$, the Boltzmann constant $k_B = 1$, and measure all energies in the unit of U unless it is otherwise mentioned.

To simulate the BHM (1) on a 2D square lattice, we will adopt the CMF method which was first introduced to study correlated spins and bosonic systems at zero temperature primarily to compute the phase boundaries [60–65]. More recently, it has been used to investigate the extended BHM in regular and frustrated lattices [66, 67], as well as to study dynamics of interacting spin systems [68, 69]. Here we extend the method to study the behavior around the SF-MI QCP of the 2D BHM as a function of temperature.

2.2 Cluster mean-field theory

In CMF theory, the entire lattice is decomposed into clusters $\mathcal{C}_1, \mathcal{C}_2, \dots$ as depicted in Fig. 1 (a) for the example of 2×2 clusters in a 2D lattice. For a cluster \mathcal{C}_i the field operators on neighboring clusters \hat{a}_j , $j \notin \mathcal{C}_i$, are approximated by their thermal averages,

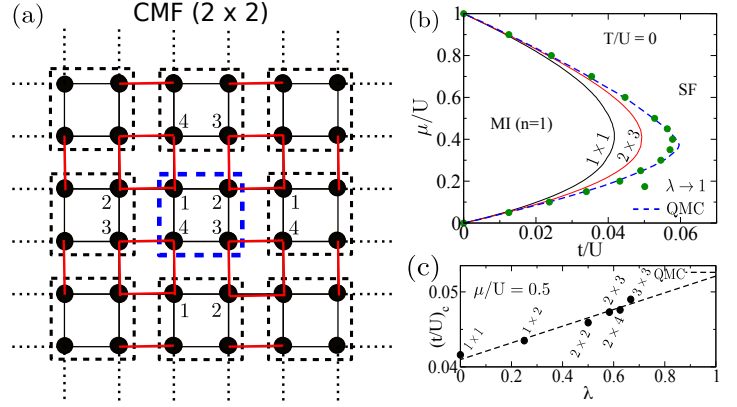


Figure 1: (color online) (a) Schematic demonstration of the CMF method in a square lattice split up into 2×2 clusters (boxes with dashed lines). The red lines show the bonds between neighboring clusters. See the text for details of the construction. (b) Zero-temperature phase diagram of the 2D BHM obtained using different cluster sizes as indicated. The critical $(t/U)_c$ in the thermodynamic limit (filled circles), extracted from the cluster finite-size scaling, are compared with QMC results of Ref. [31] (dashed line). An example of such extrapolation for $\mu/U = 0.5$ is shown in (c).

i.e., the local condensate amplitude, computed with the CMF density matrix to be determined below. This leads to the CMF Hamiltonian $\hat{\mathcal{H}} = \sum_i \hat{\mathcal{H}}_{\mathcal{C}_i}$ which is the sum of cluster Hamiltonians,

$$\begin{aligned} \hat{\mathcal{H}}_{\mathcal{C}_i} = & -t \left[\sum_{\substack{\langle i,j \rangle \\ i,j \in \mathcal{C}_i}} \hat{a}_i^\dagger \hat{a}_j + \sum_{\substack{\langle i,j \rangle \\ i \in \mathcal{C}_i, j \notin \mathcal{C}_i}} \hat{a}_i^\dagger \langle \hat{a}_j \rangle \right] + \text{h.c.} \\ & - \sum_{i \in \mathcal{C}_i} \left[\mu \hat{n}_i + \frac{U}{2} \hat{n}_i (\hat{n}_i - 1) \right]. \end{aligned} \quad (2)$$

Accordingly, the total CMF density matrix factorizes,

$$\hat{\rho} = \prod_i \hat{\rho}_{\mathcal{C}_i}, \quad \hat{\rho}_{\mathcal{C}_i} = e^{-\beta \hat{\mathcal{H}}_{\mathcal{C}_i}} / \mathcal{Z}_{\mathcal{C}}, \quad (3)$$

where $\hat{\rho}_{\mathcal{C}_i}$ is the thermal density matrix of cluster \mathcal{C}_i at the inverse temperature $\beta = 1/T$, and $\mathcal{Z}_{\mathcal{C}} = \text{Tr} \hat{\rho}_{\mathcal{C}_i}$ is the corresponding partition function of the cluster. Because of translation symmetry, the local condensate amplitude on neighboring cluster sites, $\langle \hat{a}_j \rangle$, $j \notin \mathcal{C}_i$, are identical to those on sites inside the cluster \mathcal{C}_i , shifted by one cluster length as indicated by the site numbers in Fig. 1 (a). The cluster Hamiltonian in Eq. (2) is, thus, solved by exact diagonalization and self-consistently computing the thermal averages $\langle \hat{a}_j \rangle = \text{Tr}(\hat{a}_j \hat{\rho})$ in Eqs. (2) using Eqs. (2) and (3). After self-consistent diagonalization, any CMF thermal expectation value can be calculated as $\langle \cdot \rangle = \text{Tr}(\cdot \hat{\rho})$. One can also compute the total free energy for a cluster from $F = -T \ln \mathcal{Z}_{\mathcal{C}}$ and derive thermodynamic expectation values from it.

The relevant quantities which characterize the superfluid at zero temperature are the finite condensate amplitude α_{SF} and the finite compressibility κ , defined as follows,

$$\alpha_{\text{SF}} = \frac{1}{N_{\mathcal{C}}} \sum_{i \in \mathcal{C}} |\langle \hat{a}_i \rangle|, \quad \kappa = \frac{1}{\bar{n}^2} \frac{\partial \bar{n}}{\partial \mu}, \quad (4)$$

where the average particle density is, $\bar{n} = (1/N_{\mathcal{C}}) \sum_{i \in \mathcal{C}} \langle \hat{n}_i \rangle$, and $N_{\mathcal{C}}$ is the number of lattice sites within a cluster \mathcal{C} . However, in

two dimensions at finite temperature, due to the logarithmic decay of correlation functions with distance, the condensate amplitude vanishes in the thermodynamic limit [73,74] and, therefore, cannot be used as an order parameter of the SF phase. A physical quantity which does characterize the superfluid, both at zero and finite temperatures, is the SF density ρ_s . CMF theory, like other MF theories, yields a condensate amplitude α_{SF} which remains finite in the superfluid, and vanishes at the same transition line to the MI or NF phase, where the SF density ρ_s vanishes, see Fig. 5. In the following, for simplicity we will therefore use α_{SF} to characterize the SF-MI/NF boundary at zero/finite temperature.

The zero-temperature phase diagram of the BHM in 2D is shown in Fig. 1 (b). It consists of two distinct phases – an incompressible Mott insulator, and a compressible superfluid. Noticeably, with increasing cluster size, the MI-SF phase boundary is improved over the single-site MF theory obtained simply by using a 1×1 cluster. For infinite cluster size (thermodynamic limit), the number of bonds in the cluster is given by $N_b = N_C z_c / 2$, where z_c is the lattice coordination number ($z_c = 4$ for the 2D square lattice). Therefore, we employ cluster size scaling of data with the parameter $\lambda = N_b / (N_C z_c / 2)$ as introduced in Ref. [61], and extract the values in the thermodynamic limit by extrapolating to $\lambda \rightarrow 1$, see Fig. 1 (c). The extrapolated critical hopping $(t/U)_c$ for the MI-SF transition is plotted as a function of μ/U in Fig. 1 (b) which agrees well with the QMC result. The zero-temperature phase diagram within CMF method has been analyzed in more detail in Ref. [60,62]. Physical results shown in this article will represent this extrapolation to infinite cluster size limit, $\lambda \rightarrow 1$, unless indicated otherwise.

Fock space truncation and numerical accuracy. Since for bosonic systems the occupation numbers in the canonical ensemble are unlimited, in representing and diagonalizing the Hamiltonian in Eqs. (2), (3), the Hilbert space dimension must be truncated not only by cluster size but also by the Fock space dimension. We restrict the local occupation number on any site to at most $n_i = 2$. Since higher occupation numbers are exponentially suppressed with $n_i(n_i - 1)U/T$, this approximation turns out to be sufficient for low temperatures $T/U \lesssim 0.1$ near the QCP, see Appendix A for details. For clusters up to 2×3 , the full Hamiltonian matrix is diagonalized exactly. For faster diagonalization and convergence of larger clusters at low temperatures, we use a Lanczos algorithm to compute the ν_{max} lowest-lying eigenstates. For each cluster and temperature, ν_{max} is determined such that the contribution of the higher-energy eigenstates to the partition function is less than $\mathcal{O}(10^{-8})$, $\exp[-\beta E_{\nu_{\text{max}}}] / \tilde{Z}_C < 10^{-8}$, where $\tilde{Z}_C = \sum_{\nu=1}^{\nu_{\text{max}}} \exp[-\beta E_{\nu}]$ is the truncated partition function. For instance, for $T/U = 0.1$ we find that $\sim 20\%$ of the lowest lying states are sufficient to satisfy this criterion. The computations for fixed density $\bar{n} = 1$ discussed in Sec. 4 require an additional self-consistency to adjust the chemical potential accordingly. This can substantially increase the computation time, but does in principle not limit the numerical accuracy.

3 Finite temperature phase diagram away from particle-hole symmetry

At a finite temperature, in addition to the MI and SF another phase appears, the normal fluid (NF), characterized by a vanishing superfluid density ρ_s and vanishing condensate amplitude

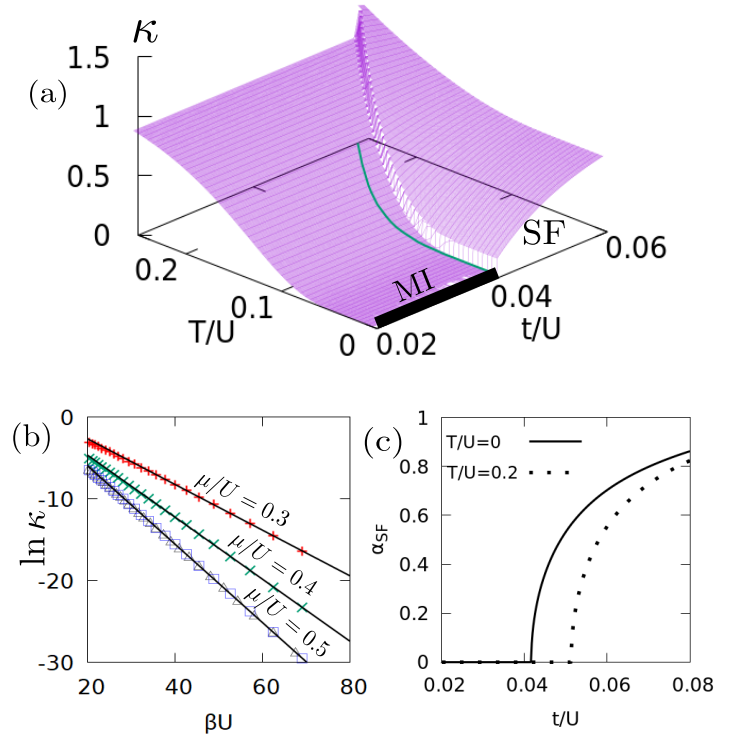


Figure 2: (Color online) Single-site MF results. (a) Compressibility κ as a function of t/U and T/U exhibiting a jump at the SF-NF boundary where the condensate amplitude α_{SF} vanishes (marked by the solid line in the $t/U - T/U$ plane). (b) Semi-log plot of κ vs βU at $t/U = 0$. The linear fits for each μ/U are shown by the solid lines. In single-site MF, the slope Δ_{ph}/U does not change with t/U as evident from overlapping data of $t/U = 0$ (open squares) and $t/U = 0.01$ (open triangles) at $\mu/U = 0.5$. (c) The variation of α_{SF} with t/U at sections $T/U = 0$ and $T/U = 0.2$ is shown. In all plots except panel (b) we set a typical value of the chemical potential $\mu/U = 0.5$, which is away from the p-h symmetry ($t/U \neq 0$).

α_{SF} , but finite compressibility κ . In two dimension the transition from superfluid to normal fluid belongs to the Berezinskii–Kosterlitz–Thouless (BKT) universality class corresponding to a vortex binding-unbinding transition [70–72]. The study of BKT physics and its associated scaling behavior discussed in Refs. [75–79], is beyond the scope of the present study, as it requires significantly larger system sizes of at least order of the vortex radius. Nevertheless, the CMF theory gives an overall correct description except for the critical region where BKT physics sets in. In the subsequent sections, we will show that it describes the phase transition line near the QCP in quantitative agreement with QMC.

Another characteristics of the SF and NF phases are the total number fluctuations $\langle \delta \hat{N}^2 \rangle$. Since the total number operator is $\hat{N} = \sum_i \hat{n}_i$, this involves non-local density correlations $\langle \hat{n}_i \hat{n}_j \rangle$. In Refs. [54,56] a relation between κ and $\langle \delta \hat{N}^2 \rangle$ via the fluctuation-dissipation theorem (FDT) has been studied in order to explore the thermometry of 2D BHM. While single-site MF theory incorporates only local number fluctuations, $\langle \delta \hat{n}_i^2 \rangle = \langle \hat{n}_i^2 \rangle - \langle \hat{n}_i \rangle^2$, the finite cluster mean-field theory does capture the non-local contributions as presented below.

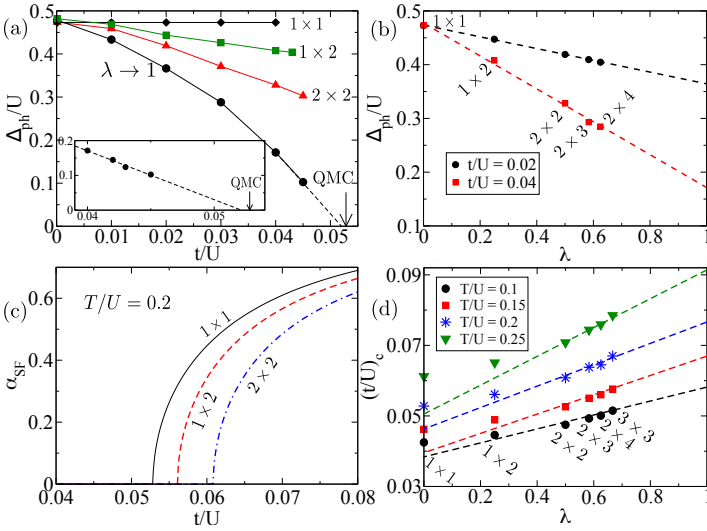


Figure 3: (Color online) (a) The particle or hole gap Δ_{ph}/U in the MI at $T = 0$, and (c) the condensate amplitude α_{SF} in the SF are plotted as a function of t/U for increasing cluster sizes. The infinite-cluster-size extrapolations of Δ_{ph}/U and of the critical hopping $(t/U)_c$ for SF-NF transition are shown in (b) and (d), respectively. The inset in (a) shows the linear behavior of Δ_{ph}/U extracted at $\lambda \rightarrow 1$ and its linear extrapolation to the MI-SF transition. From its linear fitting the critical hopping where Δ_{ph}/U vanishes is determined as $(t/U)_c \approx 0.0519$ at $T/U = 0$.

3.1 Single-site mean-field results

The MF phase diagram is shown in Fig. 2 (a). At zero temperature, the SF-MI transition with vanishing compressibility κ in the MI phase is visible, which turns into a SF-NF transition at any finite $T > 0$. The SF-NF boundary is depicted by the solid line in the $t/U - T/U$ plane in Fig. 2 (a). Here and in the following we denote the distance to the QCP by $\delta = (t/U) - (t/U)_c$. Within MF, at the critical value $(t/U)_c$, the condensate amplitude α_{SF} vanishes as $\sim |\delta|^{1/2}$ [see Fig. 2 (c)], whereas the response quantity compressibility κ exhibits a jump [see Fig. 2 (a)], indicating a second-order phase transition for any $T \geq 0$. At $T = 0$, the magnitude of the jump can be analytically estimated by perturbation theory [20]. On the MI side, upon increasing temperature a crossover to the NF occurs, exhibiting an exponential increase of $\kappa \sim \exp(-\beta\Delta_{\text{ph}})$ due to thermal activation. Here, Δ_{ph} is the minimum energy for adding or removing a particle, that is, the particle or hole gap of the Mott insulator, whichever is smaller. Fig. 2 (b) shows a logarithmic plot of κ as a function of βU for different chemical potentials μ/U . A linear fit of the data allows to extract Δ_{ph}/U for each μ/U in the limit $\beta U \gg 1$ [see Fig. 2 (b)]. It is not surprising that the single-site MF theory can give the correct particle or hole gap only in the atomic limit $t/U = 0$, namely, $\Delta_{\text{ph}}/U = (1 - \mu/U)$ and μ/U , respectively. At finite t/U , the effect of non-local density fluctuations on Δ_{ph}/U is not captured. Thus Δ_{ph}/U does not change with t/U as illustrated in Fig. 2 (b) for $t/U = 0$ and 0.01. In the next section, we will analyze the variation of Δ_{ph}/U with t/U using a finite-cluster calculation, and will set this p-h excitation energy scale as the crossover temperature between the MI and the NF.

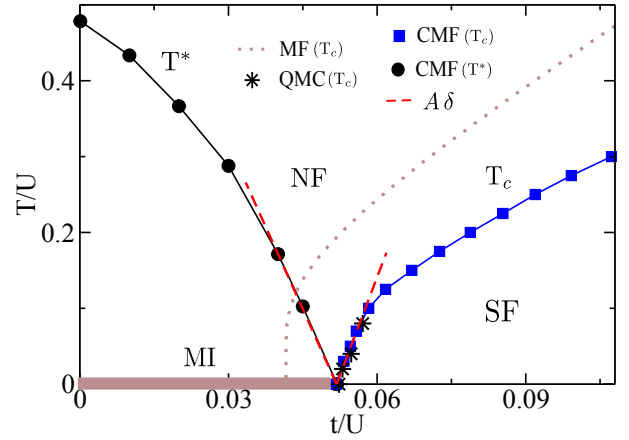


Figure 4: (Color online) Generic finite-temperature phase diagram of the 2D BHM for a fixed chemical potential $\mu/U = 0.5$. The MI phase at $T/U = 0$ is marked by the bold line on the horizontal axis. The crossover temperature T^* is set by the particle or hole gap of the Mott insulator. The SF-NF boundary T_c is obtained from the vanishing of α_{SF} (see also section 3.3). All the data presented here are obtained from infinite cluster size extrapolation shown in Fig. 3. The red dashed lines are linear fits of the data indicating a linear vanishing of T^*/U and T_c/U near the QCP. QMC data (*) from Ref. [33] and MF results (grey dotted curve) are shown for comparison.

3.2 Non-local correlation effects near QCP

As has been shown in Refs. [54, 56], non-local correlations contribute to the compressibility via the FDT and are, thus, expected to influence Δ_{ph}/U as well. In a finite-cluster calculation, intersite correlations such as $\langle \hat{n}_i \hat{n}_j \rangle$, $i, j \in \mathcal{C}$, are taken into account. In Fig. 3 (a) and (c) we show the particle or hole gap Δ_{ph}/U , whichever is smaller, and the condensate amplitude α_{SF} , respectively, as a function of t/U for several cluster sizes. We take the thermodynamic limit by the infinite-cluster extrapolation $\lambda \rightarrow 1$, as illustrated for Δ_{ph}/U as well as for $(t/U)_c$ (where α_{SF} vanishes) in Fig. 3 (b) and (d), respectively. It is clearly seen that Δ_{ph}/U depends on t/U even within the MI and NF phases where $\alpha_{\text{SF}} = 0$. As the MI-SF QCP is approached, calculating Δ_{ph}/U would require larger and larger clusters as the correlation length diverges. We observe, however, that for its smallest values Δ_{ph}/U depends linearly on t/U [see inset of Fig. 3 (a)]. Therefore, we may extrapolate Δ_{ph}/U linearly to zero. The QCP determined in this way both from the MI side (vanishing of Δ_{ph}/U) and from the SF side (vanishing of α_{SF} at $T = 0$) in the $\lambda \rightarrow 1$ limit is found to be at $(t/U)_c \approx 0.0519$. Notably, this is in close agreement with the QMC result $(t/U)_c \approx 0.0524$, marked by an arrowhead in Fig. 3 (a,d). The linear vanishing of Δ_{ph}/U can be understood from the behavior

$$\Delta_{\text{ph}}/U \sim |\delta|^{z\nu}, \quad (5)$$

with $z\nu = 1$ as expected from a generic MI-SF transition away from p-h symmetry. Here, z is the dynamical critical exponent, and ν the correlation-length exponent.

We extend the calculations to finite temperature in order to determine the SF-NF boundary in the thermodynamic limit from the vanishing of condensate amplitude, followed by the cluster finite-size scaling, $\lambda \rightarrow 1$, in the same spirit as the zero-temperature CMF calculations performed in Ref. [61]. The extension of the calcula-

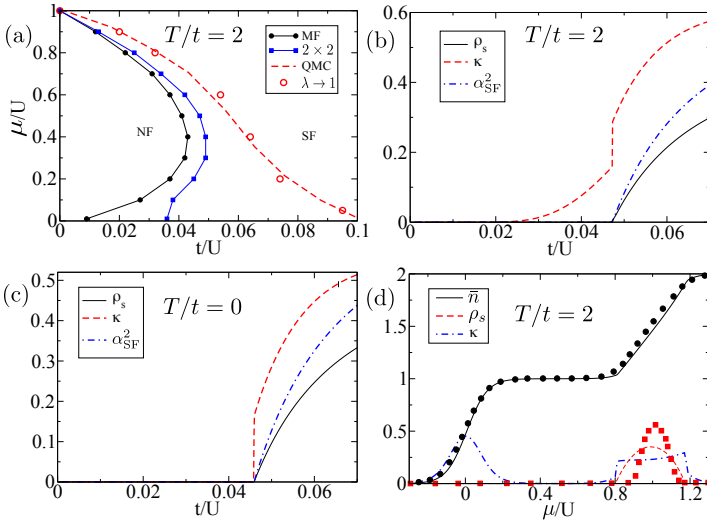


Figure 5: (Color online) (a) SF-NF phase boundary of the 2D BHM in the $t/U - \mu/U$ plane at a finite temperature $T/t = 2$ for different cluster sizes including MF and $\lambda \rightarrow 1$ extrapolation. (b, c) The compressibility κ , SF density ρ_s and squared condensate amplitude α_{SF}^2 vs. t/U for $\mu/U = 0.5$ at $T/t = 2$ and $T/t = 0$ respectively. (d) Average density \bar{n} , κ , and ρ_s as a function of μ/U at fixed $t/U = 0.025$ and $T/t = 2$. The plateau marks the first Mott lobe. For (b-d) we have used a typical cluster size 2×2 . Open circles in (a) and filled symbols in (d) are QMC data extracted from Ref. [33].

tions to finite temperature are shown in Figs. 3 (c, d). The linear extrapolation of $(t/U)_c$ for different clusters, as shown in Fig. 3 (d), is performed including the clusters up to 2×4 (where the single-site MF value is excluded). Additional $(t/U)_c$ data points obtained from a 3×3 cluster lie on the respective fitted (dashed) lines which confirms the accuracy of the extrapolation. Therefore, we will confine the extrapolation procedure to clusters of size up to 2×4 in the following.

Very close to the QCP, the behavior of T_c/U is difficult to capture, however, from our $\lambda \rightarrow 1$ extrapolated data we observe that T_c/U vanishes linearly with δ as the MI-SF transition point is approached, see Fig. 4. Such a linear behavior has also been demonstrated experimentally near the quantum critical point for a vacuum-to-superfluid transition [12]. On the MI side, we define the crossover temperature T^*/U between MI and NF as the $\lambda \rightarrow 1$ extrapolated particle or hole gap Δ_{ph}/U . A true Mott insulator with vanishing compressibility κ only exists at $T/U = 0$. The complete phase diagram is shown in Fig. 4. We note in passing that the particle (hole) gap can also be extracted by measuring the distance of a point inside the Mott lobe from its upper (lower) boundary at a fixed t/U , see the zero-temperature phase diagram in Fig. 1 (b). The results of the CMF theory may be verified experimentally by the quantum gas microscopy technique [8, 9], since it allows the measurement of non-local density correlations [14].

3.3 Superfluid fraction and sound velocity in SF phase

In an interacting Bose gas, the superfluid transport is characterized by the superfluid density rather than the condensate amplitude. It can be computed by imposing a phase gradient, which is accomplished by substituting the hopping amplitude t by $t_{ij}e^{i\theta}$ in Eq. (1),

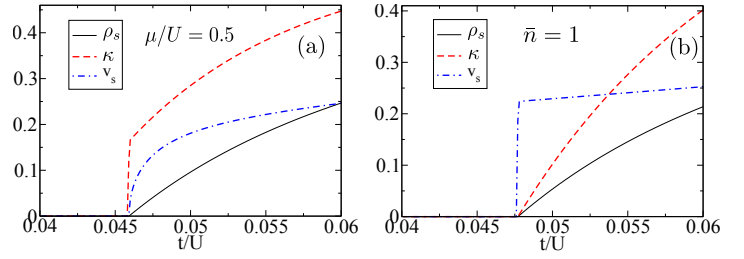


Figure 6: (Color online) Compressibility κ , superfluid density ρ_s , and sound velocity v_s vs. t/U across (a) a generic MI-SF transition for $\mu/U = 0.5$ and (b) across the p-h symmetric Mott tip for a constant density $\bar{n} = 1$. The results are shown for a typical 2×2 cluster.

where i, j are nearest neighbor sites in x direction and θ is the twist per lattice site [80]. Within CMF theory and assuming homogeneity of the system, the energy of the twisted Hamiltonian can be calculated from a representative cluster \mathcal{C} only, which yields the following expression for the SF density [81],

$$\rho_s = \frac{F(\theta) - F(0)}{N_C t \theta^2}, \quad F(\theta) = -T \ln \mathcal{Z}_C(\theta) \quad (6)$$

where $F(\theta)$ and $\mathcal{Z}_C = \sum_{\nu} \exp[-\beta E_{\nu}(\theta)]$ are the free energy and the cluster partition function, respectively, corresponding to the phase-twisted cluster Hamiltonian $\hat{\mathcal{H}}_C(\theta)$ with twist angle θ as defined above. The eigenvalues $E_{\nu}(\theta)$ of $\hat{\mathcal{H}}_C(\theta)$ can be calculated using the unperturbed eigenstates $|\nu\rangle$ of $\hat{\mathcal{H}}_C(0)$ by means of perturbation theory [81],

$$E_{\nu}(\theta) = E_{\nu}(0) + \theta^2 \sum_{\nu' \neq \nu} \frac{|\langle \nu | \hat{J} | \nu' \rangle|^2}{E_{\nu}(0) - E_{\nu'}(0)} - \frac{\theta^2}{2} \langle \nu | \hat{T} | \nu \rangle \quad (7)$$

where \hat{J} and \hat{T} are the current and kinetic energy operators, respectively, which are defined within CMF theory as follows.

$$\hat{J} = it \left[\sum_{\langle i,j \rangle \in \mathcal{C}} \hat{a}_i^{\dagger} \hat{a}_j + \sum_{\langle i,j \rangle, i \in \mathcal{C}, j \notin \mathcal{C}} \hat{a}_i^{\dagger} \langle \hat{a}_j \rangle - \text{h.c.} \right] \quad (8)$$

$$\hat{T} = t \left[\sum_{\langle i,j \rangle \in \mathcal{C}} \hat{a}_i^{\dagger} \hat{a}_j + \sum_{\langle i,j \rangle, i \in \mathcal{C}, j \notin \mathcal{C}} \hat{a}_i^{\dagger} \langle \hat{a}_j \rangle + \text{h.c.} \right] \quad (9)$$

We note that within CMF theory in the pure (non-disordered) BHM the SF density ρ_s vanishes simultaneously with α_{SF} at the transition to the MI or NF phase [Fig. 5(b,c)].

At the BKT transition in the thermodynamic limit ρ_s has a discontinuous jump, while the compressibility κ exhibits a kink [55, 78]. In CMF theory, because vortex fluctuations are not taken into account, ρ_s vanishes linearly, while compressibility exhibits a jump at the SF-NF boundary even at finite temperature, as shown in Fig. 5 (b). Based on the vanishing of ρ_s , or equivalently α_{SF} , we obtain a phase diagram in the $\mu/U - t/U$ plane at a finite temperature, shown in Fig. 5 (a). Clearly, the CMF method, after performing the $\lambda \rightarrow 1$ extrapolation, produces the phase boundary in quantitative agreement with the QMC, see also Fig. 4. Thus, it appears to give an overall correct description, except for the critical region of the BKT transition.

A true incompressible Mott insulator exists only at zero temperature where both κ and ρ_s vanish [Fig. 5 (c)]. In Fig. 5 (d) we

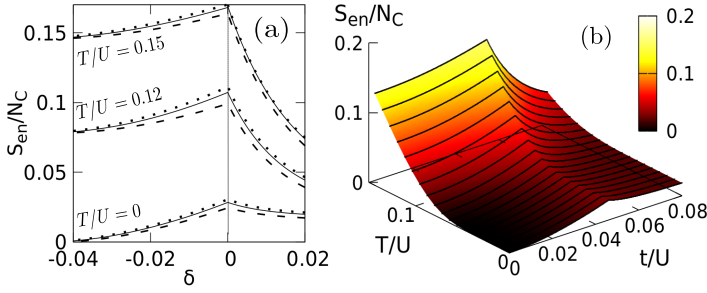


Figure 7: (Color online) (a) CMF theory results for the cluster entanglement entropy per site, S_{en}/N_C , as a function of $\delta = (t/U) - (t/U)_c$ for three different clusters, 1×2 (dashed line), 2×2 (solid line) and 2×3 (dotted line) at $\mu/U = 0.5$, and for temperatures T/U as shown. (b) Temperature dependence of S_{en}/N_C for a representative 2×2 cluster across the SF-NF transition.

also plot the average boson density \bar{n} , SF density ρ_s and compressibility κ versus μ/U for a small hopping $t/U = 0.025$ and a typical 2×2 cluster. Since the effect of correlations is less for small t/U , we indeed observe a good quantitative agreement with QMC even with a finite cluster. However, for larger t/U and a 2×2 cluster the agreement is not as good any more.

Another characteristics of a superfluid with short-range interaction is the presence of Goldstone mode which gives rise to sound modes with finite velocity. The sound velocity is related to the SF fraction and compressibility by a relation [15],

$$v_s = \sqrt{\frac{\rho_s}{m\kappa\bar{n}^2}}, \quad (10)$$

where $m = 1/2t$ is the boson effective mass in the lattice. Fig. 6 (a) shows ρ_s , κ , and the resulting v_s as a function of t/U at $T = 0$ near a generic, non-p-h symmetric MI-SF transition. Within the CMF method the sound velocity vanishes $v_s \sim \sqrt{|\delta|}$, since ρ_s vanishes linearly, but κ remains finite.

3.4 Entanglement entropy

In a many-body system, entanglement plays a crucial role in many contexts, especially near phase transitions where fluctuations are enhanced. In order to further characterize the SF-NF transition, we compute the bipartite entanglement entropy of a cluster, termed, *cluster entanglement entropy* (CEE), using CMF theory at finite temperature. It can be noted that such a calculation necessarily includes the thermal contribution since the density matrix depends on temperature [82–84]. It is defined in the following way. The finite cluster is divided into two parts, A and B , which allows us to write down any state vector in the cluster, e.g., an eigenstate $|\nu\rangle$ of \hat{H}_C as [85],

$$|\nu\rangle = \sum_{\alpha,\beta} C_\nu^{\alpha\beta} |\alpha\rangle \otimes |\beta\rangle \quad (11)$$

where $\{|\alpha\rangle\}$ ($\{|\beta\rangle\}$) is a set of basis states of the A (B) subspaces, and the matrix of expansion coefficients C_ν has dimension \sqrt{N} , N being the dimension of \hat{H}_C . To obtain the CEE at temperature T , we calculate the reduced density matrix of, say, subsystem A ,

$$\hat{\rho}^A = \text{Tr}_B(\hat{\rho}_C), \quad \hat{\rho}_C = \frac{1}{Z_C} \sum_\nu e^{-E_\nu/T} |\nu\rangle\langle\nu|, \quad (12)$$

where Tr_B is the trace over subsystem B . Inserting Eq. (11) into Eq. (12) we obtain the following expression for $\hat{\rho}^A$ and finally for the von Neumann CEE S_{en} ,

$$(\hat{\rho}^A)^{\alpha\alpha'} = \sum_\nu \sum_\beta C_\nu^{\alpha\beta} C_\nu^{\beta\alpha'*} e^{-E_\nu/T} \quad (13)$$

$$S_{\text{en}} = -\text{Tr}(\hat{\rho}^A \ln \hat{\rho}^A) \quad (14)$$

Since the entropy is an extensive quantity, the CEE per lattice site should be essentially independent of cluster size and should, therefore, represent the bipartite entanglement entropy per site (entropy density) of the macroscopic lattice. This is confirmed in Fig. 7 (a), where the CEE per lattice site is shown across the SF-NF transition as function of $\delta = (t/U) - (t/U)_c$ for three different cluster sizes and three different temperatures. The enhancement at the phase transition is clearly seen, even though BKT physics is not accounted for. The small deviations for different cluster sizes may be attributed to surface effects induced by sites located at the cluster surface. In Fig. 7 (b) we show the full temperature dependence of the CEE per site as a function of t/U for a 2×2 cluster which may be considered representative for the entanglement entropy of the macroscopic lattice and thus relevant for experimental entropy measurements which have become possible using quantum gas microscopy [13, 14].

4 Finite temperature behavior at particle-hole symmetry

We now focus on the line in parameter space where p-h symmetry is valid. Within the MI phase, at p-h symmetry, the particle gap and the hole gap are degenerate, so that particle and hole fluctuations cancel each other. Therefore, at the p-h symmetric point the MI-SF transition is not driven by density fluctuations, and a different universality class than for a generic MI-SF transition may be expected [31]. The p-h symmetric line is characterized by the particle number per site being $\bar{n} = 1$ while t/U is varied. We realize this condition at any finite temperature $T > 0$ by appropriately tuning the chemical potential μ/U in the grand-canonical ensemble. In the Mott phase at $T = 0$, where $\bar{n} = 1$ within a finite area (the Mott lobe) in the $t/U - \mu/U$ phase diagram, the p-h symmetric line is obtained in the limit $T \rightarrow 0$. It thus starts in the $\bar{n} = 1$ Mott lobe at $t/U = 0$ (atomic limit) with $\mu/U = 0.5$ and intersects at the tip of the Mott lobe.

4.1 Degenerate particle and hole excitations in the Mott phase

First, we discuss the behavior along the p-h symmetric line within the Mott lobe. We extract the gap of particle and hole excitations from the temperature dependence of the compressibility as in Sec. 3 (c.f. Fig. 2). This defines the crossover temperature $T^* = \Delta_{\text{ph}}$ between the MI and NF phases. In Fig. 8 (a) we show the particle or hole gap Δ_{ph}/U , extrapolated to the thermodynamic limit ($\lambda \rightarrow 1$) as a function of chemical potential μ/U for $\bar{n} = 1$ at fixed hopping t/U and temperature $T = 0$. The results are in good agreement with QMC data. $\Delta_{\text{ph}}(\mu)$ reaches its maximum value at the p-h symmetric point. In experiments, the particle-hole excitation gap Δ_g is directly accessible [49], while the energy for adding or removing a particle, Δ_{ph} , is not. Since Δ_g is the sum of the energies

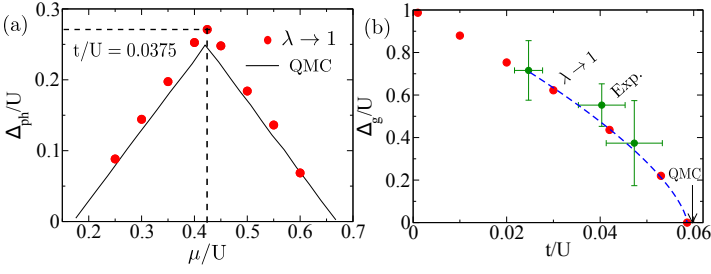


Figure 8: (Color online) Particle and hole excitations at the tip of the $\bar{n} = 1$ Mott lobe. (a) Particle or hole gap Δ_{ph}/U as a function of μ/U for $t/U = 0.0375$ in comparison to QMC results [31, 56]. The dashed lines mark the p-h symmetric value of degenerate Δ_{ph}/U . (b) Mott gap Δ_g/U as a function of t/U . Red dots: CMF results in the thermodynamic limit $\lambda \rightarrow 1$; green dots with error bars: experimental results from Ref. [49]; arrowhead: QMC result from Ref. [31]. The $\lambda \rightarrow 1$ CMF prediction for the transition point, $(t/U)_c \approx 0.0578$ is in good agreement with the QMC result of $(t/U)_c \approx 0.0597$ marked by ‘ \downarrow ’. The dashed line is a fit of $A\delta^\nu$ to the CMF data with $\nu = 0.6715$ (see text for details).

for subtracting and adding a particle, on the p-h symmetric line it is just $\Delta_g/U = 2\Delta_{ph}/U$. In Fig. 8 (b) we plot Δ_g/U as a function of t/U along the p-h symmetric line ($\bar{n} = 1$), compared with experimental data as indicated. It should be noted that, unlike at a generic MI-SF transition away from particle-hole symmetry, at the tip of the Mott lobe Δ_g does not vanish linearly. Instead, since in this case the dynamic critical exponent is $z = 1$, Δ_g/U must vanish $\sim \delta^\nu$ [c.f. Eq. 5], where the correlation-length exponent has been determined in Ref. [31] by QMC for the 2D BHM as $\nu = 0.6715$. We, thus, fit the Mott gap with a function $A\delta^\nu$, where A is a fit parameter and $\nu = 0.6715$. The fitted line is also plotted in Fig. 8 (b).

4.2 SF-NF transition and phase diagram for $\bar{n} = 1$

To complete the phase diagram we now study the SF-NF transition with increasing temperature, keeping the average density fixed at $\bar{n} = 1$. The phase diagram is shown in Fig. 9. The right part shows the critical temperature T_c/U line where the condensate amplitude vanishes in the infinite-cluster limit $\lambda \rightarrow 1$. The crossover line between MI and NF on the left is obtained as the particle or hole gap Δ_{ph} of the MI at their degeneracy point as discussed in Sec. 4.1, c.f. Fig. 8 (b). Fig. 9 also shows QMC [31] and B-DMFT results [35] for comparison. The striking improvement of CMF over MF theory is clearly seen, particularly, the CMF results are consistent with the vanishing of T^*/U as well as T_c/U with an exponent of 0.6715 [31] at the QCP, shown as the red, dashed lines.

For the p-h symmetric MI-SF transition (tip of the Mott lobe) both the compressibility κ and the superfluid fraction ρ_s vanish at the QCP linearly with δ as shown using a typical 2×2 cluster [see Fig. 6 (b)]. It follows from Eq. (10) that the sound velocity of the superfluid remains finite, in contrast to a generic transition away from p-h symmetry as discussed in Sec. 3.3, c.f. Fig. 6 (a).

5 Summary and conclusion

Remarkably, the contrasting behavior of T_c/U between the two universality classes are well captured within CMF theory after per-

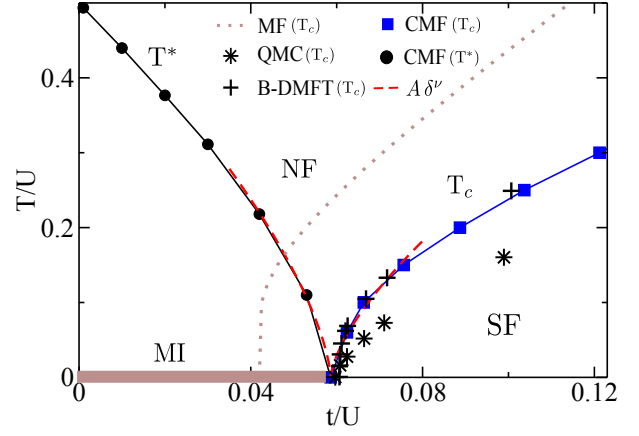


Figure 9: (Color online) Finite-temperature phase diagram of the 2D BHM for fixed average density $\bar{n} = 1$. The MI phase at $T/U = 0$ is marked by a bold line on the t/U axis. The CMF results for the MI-NF crossover temperature $T^* = \Delta_{ph}$ and the SF-NF transition temperature T_c are shown as black circles and blue squares, respectively. QMC data (*) from Ref. [31] and B-DMFT results from Ref. [35] are shown for comparison. The red, dashed lines are fits of the function $A\delta^\nu$ to our CMF data on the MI as well as the SF side of the transition. The grey, dotted curve represents the single-site MF result.

forming the cluster size extrapolation to $\lambda \rightarrow 1$.

In summary, we have computed the finite temperature phase diagram of the two-dimensional Bose Hubbard model by means of cluster mean-field (CMF) theory both for a constant chemical potential and for the p-h symmetric case of a constant density $\bar{n} = 1$. To characterize the different phases, we computed the condensate amplitude α_{SF} and superfluid density ρ_s using the CMF theory where both the quantities are finite only in the superfluid phase, and the compressibility κ which is non-zero both in the superfluid and the normal fluid, but vanishes in the Mott insulator. While the vanishing of both α_{SF} and ρ_s determines the critical temperature T_c/U for the superfluid-to-normal fluid transition, the particle or hole gap Δ_{ph} calculated from compressibility defines the crossover temperature T^*/U between Mott insulator and normal fluid. We further calculated the cluster entanglement entropy which is enhanced near the critical region and exhibits a peak at the SF-NF boundary, thereby providing an alternate way to identify the superfluid transition. We further discussed the behavior of the critical temperature T_c/U and the crossover temperature T^*/U near the quantum critical point, both at a generic MI-SF transition, i.e. for a fixed chemical potential, as well as for a particle-hole (p-h) symmetric transition which corresponds to the tip of the Mott lobe.

By increasing the cluster size, we analyzed the effect of correlation in a systematic way. Capturing the variation of the particle/hole excitation gap with hopping t/U is a direct consequence of this. We showed how the phase boundaries got improved with respect to the single-site mean field estimation. In the thermodynamic limit, achieved by performing a cluster-size-extrapolation, our results quantitatively agree with quantum Monte Carlo (QMC) data and also with experiment.

Although the critical region of BKT transition is not captured by the approach, nevertheless, it is remarkable how accurately the CMF method with infinite-cluster extrapolation reproduces the critical hopping $(t/U)_c$ and also captures the behavior of the super-

fluid critical temperature T_c and the normal-fluid crossover temperature T^* near QCP for both a generic and the p-h symmetric transition. This is an indication that much of the non-local correlations that determine the possible critical behavior are incorporated in the finite-size clusters considered here, and that dynamical fluctuations are of minor importance here.

The results of the cluster mean field theory can be tested experimentally by quantum gas microscopy [8,9] as discussed in Sec. 3.2 and in Sec. 3.4. Our study further opens up possibilities for future applications of the CMF method to investigate non-equilibrium situations like the quench dynamics across the quantum phase transition, to analyze the phases of bosons in more complicated situations like the Bose glass problem in geometrically frustrated or disordered lattices at zero or finite temperature.

A Effect of truncation on Boson number states

Since the Fock space dimension of bosons is, in principle, infinite, which is, however, truncated in any numerical calculations, therefore, it is important to justify such truncation within the regime of interest. Since our concern is the accuracy of the estimated

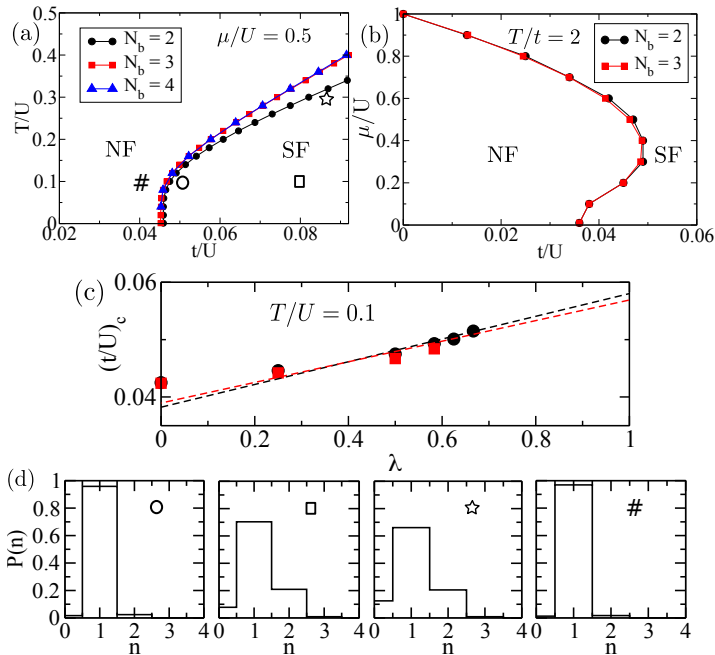


Figure 10: (Color online) (a) Phase diagram in T/U vs t/U plane is shown for a generic transition at $\mu/U = 0.5$ using different occupation number truncations N_b . In (c) $(t/U)_c$ for different clusters with $N_b = 2$ and 3 are plotted along with the $\lambda \rightarrow 1$ extrapolation for each of the cases at $T/U = 0.1$. (b) Phase diagram in $\mu/U - t/U$ plane at a finite temperature $T/t = 2$ is shown for number truncations at $N_b = 2, 3$. (d) Histogram of $P(n)$ -distribution over occupation number n in different parts of the phase diagram in (a), as marked by different symbols. The calculations in (a-d), except for (c), are performed using a typical 2×2 cluster.

phase boundary, we plot, in Fig. 10a, SF–NF phase boundaries in $T/U - t/U$ plane for different truncation in the occupation number at $N_b = 2, 3$, and 4 using a typical 2×2 cluster. Clearly, at low temperatures close to the QCP, which is the focus of the

present study, the curves do overlap for all three cases including the higher truncation, which is not the case for higher temperature, as expected. It can be noted that the fitting of T_c/U curve near QCP, as shown in Fig. 4 and 9, are done up to temperature $T/U \sim 0.1$, and at this maximum point we have overlaid the critical hopping $(t/U)_c$ for SF–NF transition using $N_b = 3$ on top of the data obtained using $N_b = 2$ occupation number truncation. For both the cases the $\lambda \rightarrow 1$ extrapolations are shown. The truncation error on the SF–NF boundary in the extrapolated $(t/U)_c$ turns out to be $\sim 2\%$ at $T/U = 0.1$, which is even smaller compared to the standard error in linear fitting. Therefore, our results near QCP, specifically, the identification of two different universality classes emerging at and away from the tip of the Mott lobe are not affected due to number truncation. In Fig. 10b we have further shown that the SF–NF boundaries in the t/U vs μ/U plane for $T/t = 2$ (see blue squares in Fig. 5a in the main text) also does not change with increasing the truncation to $N_b = 3$. Further increase in temperature $T/U \sim 0.2$, the phase boundary deviates ($\sim 5\%$ for a 2×2 cluster), as expected, however, that does not concern the critical behavior which is the main purpose of this work.

To further illustrate the effect of truncation in different parts of the phase diagram we plot the distribution $P(n)$ over the occupation number basis denoted by n in Fig. 10d. At low temperature $T/U \sim 0.1$ near the SF–NF boundary (marked by ‘o’ in SF and ‘#’ in NF) $P(2) \sim 2\%$, which justifies the truncation at $N_b = 2$ in the regime of our interest. However, away from the boundary or at higher temperature $P(2) \sim 22\%$, and therefore, a truncation at $N_b = 2$ is no longer sufficient. More precisely, at higher temperature $T/U \sim 0.3$ the phase boundary, as depicted in Fig. 10a, is shifted by $\sim 10\%$ in t/U direction. Thereby, the extrapolated values at higher temperatures are also expected to deviate.

Acknowledgements

We thank Subhasis Sinha, Axel Pelster and Anna Posazhennikova for useful discussions. This work was funded by the Deutsche Forschungsgemeinschaft (DFG, German Research Foundation) under Germany’s Excellence Strategy – Cluster of Excellence Matter and Light for Quantum Computing (ML4Q) EXC 2004/1 – 390534769, and through the DFG Collaborative Research Center CRC 185 OSCAR – 277625399. S.R. acknowledges a scholarship of the Alexander von Humboldt Foundation, Germany.

References

- [1] S. Sachdev, *Quantum Phase Transitions*, 2nd ed. (Cambridge University, Cambridge, England, 2011).
- [2] U. C. Täuber, *Phase Transitions and Scaling in Systems Far from Equilibrium*, *Annu. Rev. Condens. Matter Phys.* **2017**, 8, 185.
- [3] M. Lewenstein, A. Sanpera, and V. Ahufinger, *Ultracold Atoms in Optical Lattices* (Oxford University Press, Oxford, England, 2012).
- [4] M. E. Fisher, *The theory of equilibrium critical phenomena*, *Rep. Prog. Phys.* **1967**, 30, 615.

- [5] H. E. Stanley, *Introduction to Phase Transitions and Critical Phenomena* (Oxford, UK: Clarendon, 1971).
- [6] R. Horodecki, P. Horodecki, M. Horodecki and K. Horodecki, *Quantum entanglement*, Rev. Mod. Phys. **2009**, 81, 865.
- [7] I. Bloch, J. Dalibard, and W. Zwerger, *Many-body physics with ultracold gases*, Rev. Mod. Phys. **2008**, 80, 885.
- [8] J. F. Sherson, C. Weitenberg, M. Endres, M. Cheneau, I. Bloch and S. Kühn, *Single-atom-resolved fluorescence imaging of an atomic Mott insulator*, Nature (London) **2010**, 467, 68.
- [9] W. S. Bakr, J. I. Gillen, A. Peng, S. Fölling and M. Greiner, *A quantum gas microscope for detecting single atoms in a Hubbard-regime optical lattice*, Nature **2009**, 462, 74.
- [10] N. Gemelke, X. Zhang, C. Hung and C. Chin, *In situ observation of incompressible Mott-insulating domains in ultracold atomic gases*, Nature **2009**, 460, 995.
- [11] C.-L. Hung, X. Zhang, N. Gemelke, and C. Chin, *Observation of scale invariance and universality in two-dimensional Bose gases*, Nature (London) **2011**, 470, 236.
- [12] X. Zhang, C. Hung, S. Tung and C. Chin, *Observation of Quantum Criticality with Ultracold Atoms in Optical Lattices*, Science **2012**, 335, 1070.
- [13] R. Islam, R. Ma, P. Preiss, M. Tai, A. Lukin, M. Rispoli and M. Greiner, *Measuring entanglement entropy in a quantum many-body system*, Nature **2015**, 528, 77.
- [14] A. Lukin, M. Rispoli, R. Schittko, M. E. Tai, A. M. Kaufman, S. Choi, V. Khemani, J. Léonard and M. Greiner, *Probing entanglement in a many-body-localized system*, Science **2019**, 364, 256.
- [15] M. P. A. Fisher, P. B. Weichman, G. Grinstein and D. S. Fisher, *Boson localization and the superfluid-insulator transition*, Phys. Rev. B **1989**, 40, 546.
- [16] D. Jaksch, C. Bruder, J. I. Cirac, C. W. Gardiner and P. Zoller, *Cold Bosonic Atoms in Optical Lattices*, Phys. Rev. Lett. **1998**, 81, 3108.
- [17] M. Greiner, O. Mandel, T. Esslinger, T. W. Hänsch and I. Bloch, *Quantum phase transition from a superfluid to a Mott insulator in a gas of ultracold atoms*, Nature **2002**, 415, 39.
- [18] I. B. Spielman, W. D. Phillips and J. V. Porto, *Mott-Insulator Transition in a Two-Dimensional Atomic Bose Gas*, Phys. Rev. Lett. **2007**, 98, 080404.
- [19] K. Jiménez-García, R. L. Compton, Y.-J. Lin, W. D. Phillips, J. V. Porto and I. B. Spielman, *Phases of a Two-Dimensional Bose Gas in an Optical Lattice*, Phys. Rev. Lett. **2010**, 105, 110401.
- [20] D. Oosten, P. Straten and H. Stoof, *Quantum phases in an optical lattice*, Phys. Rev. A **2001**, 63, 053601.
- [21] J. K. Freericks and H. Monien, *Strong-coupling expansions for the pure and disordered Bose-Hubbard model*, Phys. Rev. B **1996**, 53, 2691.
- [22] M. Gupta, H. R. Krishnamurthy and J. K. Freericks, *Strong-coupling expansion for ultracold bosons in an optical lattice at finite temperatures in the presence of superfluidity*, Phys. Rev. A **2013**, 88, 053636.
- [23] F. E. A. dos Santos and A. Pelster, *Quantum phase diagram of bosons in optical lattices*, Phys. Rev. A **2009**, 79, 013614.
- [24] B. Bradlyn, F. E. A. dos Santos and A. Pelster, *Effective action approach for quantum phase transitions in bosonic lattices*, Phys. Rev. A **2009**, 79, 013615.
- [25] A. S. Sajna, T. P. Polak, R. Micnas, and P. Rozek, *Ground-state and finite-temperature properties of correlated ultracold bosons on optical lattices*, Phys. Rev. A **2015**, 92, 013602.
- [26] A. Rançon and N. Dupuis, *Nonperturbative renormalization group approach to the Bose-Hubbard model*, Phys. Rev. B **2011**, 83, 172501.
- [27] A. Rançon and N. Dupuis, *Nonperturbative renormalization group approach to strongly correlated lattice bosons*, Phys. Rev. B **2011**, 84, 174513.
- [28] A. Rançon, N. Dupuis, *Quantum XY criticality in a two-dimensional Bose gas near the Mott transition*, Europhys. Lett. **2013**, 104, 16002.
- [29] A. Rançon, O. Kodio, N. Dupuis, and P. Lecheminant, *Thermodynamics in the vicinity of a relativistic quantum critical point in $2 + 1$ dimensions*, Phys. Rev. E **2013**, 88, 012113.
- [30] B. Capogrosso-Sansone, N. V. Prokof'ev, and B. V. Svistunov, *Phase diagram and thermodynamics of the three-dimensional Bose-Hubbard model*, Phys. Rev. B **2007**, 75, 134302.
- [31] B. Capogrosso-Sansone, S. Söyler, N. Prokof'ev and B. Svistunov, *Monte Carlo study of the two-dimensional Bose-Hubbard model*, Phys. Rev. A **2008**, 77, 015602.
- [32] M. Rigol, G. G. Batrouni, V. G. Rousseau, and R. T. Scalettar, *State diagrams for harmonically trapped bosons in optical lattices*, Phys. Rev. A **2009**, 79, 053605.
- [33] K. W. Mahmud, E. N. Duchon, Y. Kato, N. Kawashima, R. T. Scalettar, and N. Trivedi, *Finite-temperature study of bosons in a two-dimensional optical lattice*, Phys. Rev. B **2011**, 84, 054302.
- [34] K. Byczuk and D. Vollhardt, *Correlated bosons on a lattice: Dynamical mean-field theory for Bose-Einstein condensed and normal phases*, Phys. Rev. B **2008**, 77, 235106.
- [35] P. Anders, E. Gull, L. Pollet, M. Troyer, and P. Werner, *Dynamical mean-field theory for bosons*, New J. Phys. **2011**, 13, 075013.
- [36] A. Dutta, C. Trefzger, and K. Sengupta, *Projection operator approach to the Bose-Hubbard model*, Phys. Rev. B **2012**, 86, 085140.
- [37] T. D. Kühner and H. Monien, *Phases of the one-dimensional Bose-Hubbard model*, Phys. Rev. B **1998**, 58, R14741(R).

- [38] T. D. Kühner, S. R. White and H. Monien, *One-dimensional Bose-Hubbard model with nearest-neighbor interaction*, Phys. Rev. B **2000**, 61, 12474.
- [39] C. Kollath, U. Schollwöck, J. von Delft, and W. Zwerger, *Spatial correlations of trapped one-dimensional bosons in an optical lattice*, Phys. Rev. A **2004**, 69, 031601(R).
- [40] C. Kollath, U. Schollwöck, J. von Delft, and W. Zwerger, *One-dimensional density waves of ultracold bosons in an optical lattice*, Phys. Rev. A **2005**, 71, 053606.
- [41] S. Ejima, H. Fehske, F. Gebhard, K. zu Munster, M. Knap, E. Arrigoni, and W. von der Linden, *Characterization of Mott-insulating and superfluid phases in the one-dimensional Bose-Hubbard model*, Phys. Rev. A **2005**, 85, 053644.
- [42] W. Krempa, E. S. Sørensen and S. Sachdev, *The dynamics of quantum criticality revealed by quantum Monte Carlo and holography*, Nat. Phys. **2014**, 10, 361.
- [43] K. Chen, L. Liu, Y. Deng, L. Pollet and N. Prokof'ev, *Universal Conductivity in a Two-Dimensional Superfluid-to-Insulator Quantum Critical System*, Phys. Rev. Lett. **2014**, 112, 030402.
- [44] N. Elstner and H. Monien, *Dynamics and thermodynamics of the Bose-Hubbard model*, Phys. Rev. B **1999**, 59, 12184.
- [45] D. B. M. Dickerscheid, D. van Oosten, P. J. H. Denteneer and H. T. C. Stoof, *Ultracold atoms in optical lattices*, Phys. Rev. A **2003**, 68, 043623.
- [46] K. Sengupta and N. Dupuis, *Mott-insulator-to-superfluid transition in the Bose-Hubbard model: A strong-coupling approach*, Phys. Rev. A **2005**, 71, 033629.
- [47] S. D. Huber, E. Altman, H. P. Büchler, and G. Blatter, *Dynamical properties of ultracold bosons in an optical lattice*, Phys. Rev. B **2007**, 75, 085106.
- [48] D. Podolsky, A. Auerbach, and D. P. Arovas, *Visibility of the amplitude (Higgs) mode in condensed matter*, Phys. Rev. B **2011**, 84, 174522.
- [49] M. Endres, T. Fukuhara, D. Pekker, M. Cheneau, P. Schauß, C. Gross, E. Demler, S. Kuhr and I. Bloch, *The 'Higgs' amplitude mode at the two-dimensional superfluid/Mott insulator transition*, Nature **2012**, 487, 454.
- [50] A. Behrle, T. Harrison, J. Kombe, K. Gao, M. Link, J.-S. Bernier, C. Kollath, and M. Köhl, *Higgs mode in a strongly interacting fermionic superfluid*, Nat. Phys. **2018**, 14, 781.
- [51] Y. Kato, Q. Zhou, N. Kawashima and N. Trivedi, *Sharp peaks in the momentum distribution of bosons in optical lattices in the normal state*, Nat. Phys. **2008**, 4, 617.
- [52] S. Hesselmann and S. Wessel, *Thermal Ising transitions in the vicinity of two-dimensional quantum critical points*, Phys. Rev. B **2016**, 93, 155157.
- [53] K. R. A. Hazzard and E. J. Mueller, *Techniques to measure quantum criticality in cold atoms*, Phys. Rev. A **2011**, 84, 013604.
- [54] S. Fang, C. Chung, P. Ma, P. Chen and D. Wang, *Quantum criticality from in situ density imaging*, Phys. Rev. A **2011**, 83, 031605(R).
- [55] E. Duchon and N. Trivedi, *Fluctuations and quantum criticality in the two-dimensional Bose Hubbard model*, Ann. Phys. (Berlin) **2013**, 525, 35.
- [56] E. Duchon, Y. Kato and N. Trivedi, *Diagnostic for phases and quantum critical regions using deviations from the local fluctuation-dissipation theorem*, Phys. Rev. A **2012**, 86, 063608.
- [57] A. Joshi and P. Majumdar, *A classical fluctuation theory of the superfluid, Mott, and normal phases of correlated bosons*, Eur. Phys. J. B **2020**, 93, 33.
- [58] M. O. C. Pires, and E. J. V. de Passos, *Superfluid to Normal Fluid Phase Transition in the Bose Gas Trapped in Two-Dimensional Optical Lattices at Finite Temperature*, Braz. J. Phys. **2017**, 47, 1.
- [59] S. Trotzky, L. Pollet, F. Gerbier, U. Schnorrberger, I. Bloch, N. V. Prokof'ev, B. Svistunov and M. Troyer, *Suppression of the critical temperature for superfluidity near the Mott transition*, Nat. Phys. **2010**, 6, 998.
- [60] D. Pekker, B. Wunsch, T. Kitagawa, E. Manousakis, A. S. Sørensen and E. Demler, *Signatures of the superfluid to Mott insulator transition in equilibrium and in dynamical ramps*, Phys. Rev. B **2012**, 86, 144527.
- [61] D. Yamamoto, A. Masaki and I. Danshita, *Quantum phases of hardcore bosons with long-range interactions on a square lattice*, Phys. Rev. B **2012**, 86, 054516.
- [62] Dirk-Sören Lühmann, *Cluster Gutzwiller method for bosonic lattice systems*, Phys. Rev. A **2013**, 87, 043619.
- [63] D. Yamamoto, I. Danshita, and Carlos A. R. Sá de Melo, *Dipolar bosons in triangular optical lattices: Quantum phase transitions and anomalous hysteresis*, Phys. Rev. A **2012**, 85, 021601(R).
- [64] P. Buonsante, V. Penna and A. Vezzani, *Analytical mean-field approach to the phase-diagram of ultracold bosons in optical superlattices*, Laser Physics **2005**, 15, 361.
- [65] K. Suthar, R. Kraus, H. Sable, D. Angom, G. Morigi and J. Zakrzewski, *Staggered superfluid phases of dipolar bosons in two-dimensional square lattices*, Phys. Rev. B **2020**, 102, 214503.
- [66] K. Suthar, H. Sable, R. Bai, S. Bandyopadhyay, S. Pal, and D. Angom, *Supersolid phase of the extended Bose-Hubbard model with an artificial gauge field*, Phys. Rev. A **2020**, 102, 013320.
- [67] M. Malakar, S. Ray, S. Sinha, and D. Angom, *Phases and collective modes of bosons in a triangular lattice at finite temperature: A cluster mean field study*, Phys. Rev. B **2020**, 102, 184515.
- [68] G. Piccitto, B. Zunkovic, and A. Silva, *Dynamical phase diagram of a quantum Ising chain with long-range interactions*, Phys. Rev. B **2019**, 100, 180402(R).

- [69] J. Jin, A. Biella, O. Viyuela, L. Mazza, J. Keeling, R. Fazio, and D. Rossini, *Cluster Mean-Field Approach to the Steady-State Phase Diagram of Dissipative Spin Systems*, Phys. Rev. X **2016**, 6, 031011.
- [70] V. L. Berezinskii, *Destruction of Long-range Order in One-dimensional and Two-dimensional Systems Possessing a Continuous Symmetry Group. II. Quantum Systems*, Sov. Phys. JETP **1972**, 34, 610.
- [71] J. M. Kosterlitz and D. J. Thouless, *Ordering, metastability and phase transitions in two-dimensional systems*, J. Phys. C **1973**, 6, 1181.
- [72] D. R. Nelson, J. M. Kosterlitz, *Universal Jump in the Superfluid Density of Two-Dimensional Superfluids*, Phys. Rev. Lett. **1977**, 39, 1201.
- [73] N. D. Mermin, and H. Wagner, *Absence of Ferromagnetism or Antiferromagnetism in One- or Two-Dimensional Isotropic Heisenberg Models*, Phys. Rev. Lett. **1966**, 17, 1133.
- [74] P. C. Hohenberg, *Existence of Long-Range Order in One and Two Dimensions*, Phys. Rev. **1967**, 158, 383.
- [75] M. Holzmann, G. Baym, J.-P. Blaizot, and F. Laloë, *Superfluid transition of homogeneous and trapped two-dimensional Bose gases*, Proc. Natl. Acad. Sci. USA **2007**, 104, 1476.
- [76] N. Prokof'ev, O. Ruebenacker, and B. Svistunov, *Critical Point of a Weakly Interacting Two-Dimensional Bose Gas*, Phys. Rev. Lett. **2001**, 87, 270402.
- [77] D. S. Petrov, M. Holzmann, and G. V. Shlyapnikov, *Bose-Einstein Condensation in Quasi-2D Trapped Gases*, Phys. Rev. Lett. **2000**, 84, 2551.
- [78] J. Carrasquilla and M. Rigol, *Superfluid to normal phase transition in strongly correlated bosons in two and three dimensions*, Phys. Rev. A **2012**, 86, 043629.
- [79] Kenji Harada and Naoki Kawashima, *Universal jump in the helicity modulus of the two-dimensional quantum XY model*, Phys. Rev. B **1997**, 55, R11949(R).
- [80] M. E. Fisher, M. N. Barber, and D. Jasnow, *Helicity Modulus, Superfluidity, and Scaling in Isotropic Systems*, Phys. Rev. A **1973**, 8, 1111.
- [81] R. Roth and K. Burnett, *Phase diagram of bosonic atoms in two-color superlattices*, Phys. Rev. A **2003**, 68, 023604.
- [82] B. Chen and J. Wu, *Single interval Rényi entropy at low temperature*, J. High Energ. **2014**, 2014, 32.
- [83] B. Swingle and T. Senthil, *Universal crossovers between entanglement entropy and thermal entropy*, Phys. Rev. B **2013**, 87, 045123.
- [84] N. Roy and S. Sinha, *A finite temperature study of ideal quantum gases in the presence of one dimensional quasi-periodic potential*, J. Stat. Mech. **2018** 053106.
- [85] U. Schollwöck, *The density-matrix renormalization group in the age of matrix product states*, Ann. Phys. (Amsterdam) **2011**, 326, 96.